Exciton Delocalization and Initial Dephasing Dynamics of Purple Bacterial LH2

L. D. Book, A. E. Ostafin,† N. Ponomarenko, J. R. Norris, and N. F. Scherer*

Department of Chemistry, the James Franck Institute and the Institute for Biophysical Dynamics, 5735 S. Ellis Avenue, University of Chicago, Chicago, Illinois 60637

Received: February 7, 2000; In Final Form: June 13, 2000

Ultrafast four-wave mixing spectroscopies are employed to study exciton dynamics associated with the B800 and B850 transitions of LH2 from *Rhodobacter sphaeroides*. Bacteriochlorophyll$_a$, the constituent chromophore of the B800 and B850 aggregates, is studied as a monomer in solution for comparison. Frequency-resolved pump−probe spectra measured across the B800 and B850 bands establish that at zero delay the transition dipole moment of B850 is substantially larger than that of B800, indicating an initial coherence size of ∼13 chromophores in the (18-member) B850 aggregate. Novel frequency-resolved stimulated photon echo measurements show that intermolecular interactions in the B850 ring reduce the coupling of this band's electronic transition to nuclear motion. In contrast, linear electron−nuclear coupling is comparable in the bacteriochlorophyll$_a$ monomer and B800, where exciton coupling is weak. Photon echo peak shift data are consistent with these observations. The initial localization dynamics of the B850 exciton are resolved with transient grating and pump−probe magic angle measurements. These data show that the enhanced transition dipole moment of B850 at the moment of excitation contracts significantly with a time constant of ∼50 fs (for transient grating) due to exciton dephasing resulting in localization. Pump−probe anisotropy measurements reveal substantial transition dipole moment orientational relaxation with nearly the same time constant. These experimental data will be useful for the development of a rigorous theoretical picture of ultrafast exciton dynamics in LH2. B850's large transition dipole moment for absorption may play an important role in the biological function of LH2, as it would enhance the energy transfer rate between B800 and B850.

I. Introduction

Photosynthetic organisms convert solar energy into chemical energy through an electrochemical potential that results from an initial light-driven charge-separation reaction that occurs in a reaction center (RC) protein. Prior to the charge-separation step, light energy must be captured and transported to the RC.[1−4] In several species of purple bacteria light absorption and transport is accomplished by two types of light harvesting antenna complexes, LH1 and LH2. The LH1 complex is closely associated with the RC; the RC is contained within the LH1 structure.[5] Circular LH2 aggregates are arranged peripherally to the LH1−RC core complex. For proper function, photons initially captured by LH2 must be funneled to LH1 and then transferred to the RC with high quantum yield. A central issue is how the highly symmetric LH1 and LH2 structures facilitate high quantum efficiency in excitation transport.

Both types of light harvesting complexes are composed of aggregates of bacteriochlorophyll (BChl) chromophores.[1] The X-ray structure of LH2 from *Rhodopseudomonas acidophila* reveals that this complex contains two rings of BChl's,[6] each of which is responsible for either the B800 or B850 band in the LH2 absorption spectrum (Figure 1a).[7] The B800 ring contains nine well-separated, weakly interacting chromophores (nearest-neighbor distance of 21 Å). The B850 ring is composed of nine closely spaced BChl dimer unit cells; the nearest neighbor distance is 9.6 Å between chromophores of the same dimer and 8.9 Å between those belonging to adjacent dimers.[8] The LH2 complex has roughly C_9 symmetry.

The close proximity of chromophores in the B850 ring means that interchromophore interactions must be taken into account to understand its spectral properties.[2,7,9,10] The BChl Q_y transition dipole moments of B850 are oriented nearly in-line in an alternating head-to-head and tail-to-tail arrangement.[8] This structural arrangement suggests that electronic coupling may be quite strong among members of the B850 ring. The resulting multichromophore interactions and the spectral shift of the absorption (ϵ_{max} of BChl$_a$ in solution is at 12800−13000 cm^{-1} versus 11750 cm^{-1} in LH2) suggest that some degree of cooperative electronic state, i.e., exciton, description is appropriate.[11] Indeed, several groups have calculated exciton exchange energies for nearest-neighbor BChl's to be in the range of 300 cm^{-1};[2,7,9,10] one electronic structure calculation has even predicted the interaction between chromophores of the same dimeric subunit to be nearly 800 cm^{-1}.[12] These strong intermolecular couplings indicate that excitons created in B850 by absorption or energy transfer processes may be delocalized over a number chromophores within the ring. Determination of the exciton coherence size in a molecular aggregate requires not only knowledge of the interchromophore interaction strength, but also information about the extent of static inhomogeneous broadening[13] and dynamic exciton-vibrational coupling[14,15] present in the complex. A rigorous definition of the exciton coherence size is given in terms of the inverse participation ratio of the exciton density matrix (see ref 15 and eqs 11 and 12 below). The coherence size should, in fact, be time-dependent;[16]

† Current address: Department of Chemical Engineering, University of Notre Dame, Notre Dame, IN 46556.

* Corresponding author. Electronic mail: nscherer@rainbow.uchicago.edu.

10.1021/jp000485d CCC: $19.00
Published on Web 08/05/2000

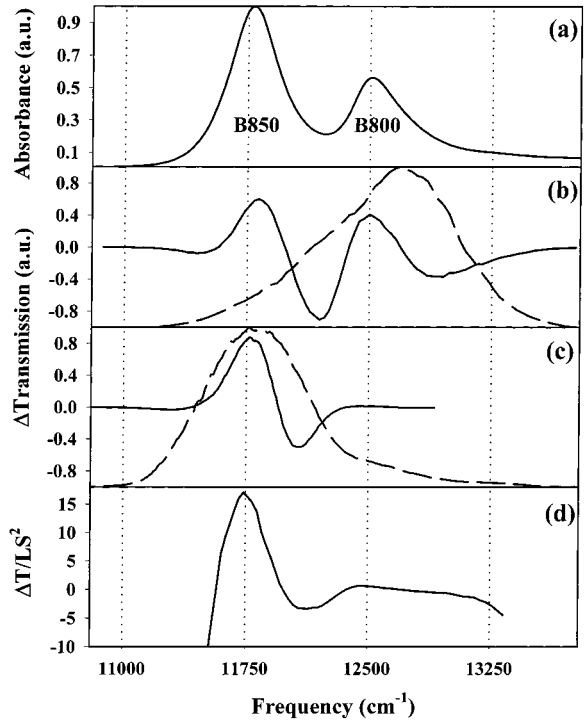

Figure 1. (a) LH2 absorption spectrum in the near-infrared. The positions of the B800 and B850 bands are indicated. (b) Frequency-resolved pump−probe signal of LH2 (solid line) with the pump and probe pulses coincident in time. The spectrum of the pulses (peak at 12650 cm^{-1}) is overlayed on the signal (dashed line). (c) Frequency-resolved pump−probe signal of LH2 (solid line) with the pump and probe pulses coincident in time. The spectrum of the pulses (peak at 11750 cm^{-1}) is overlayed on the signal (dashed line). (d) Pump−probe signal shown in (b) divided by the square of the laser spectrum (LS) used in the measurement.

in general it is not possible to characterize the exciton size of a particular aggregate with a single number.

The extent of exciton delocalization in LH complexes is a subject of widespread interest.[17] Several years ago, Reddy et al. determined from hole burning data at 1.6 K that B800 was primarily inhomogeneously broadened while the B850 band was dominated by homogeneous broadening.[18] Recent single-complex fluorescence excitation spectra have confirmed this low-temperature result.[19] This suggests that inhomogeneities among the constituent monomers of the B850 ring are averaged out by delocalization of the excitation over a number of chromophores.[20] More recently, frequency-domain nonlinear absorption measurements by Leupold et al. yielded a value of ∼25 D for the B850 transition dipole moment, about four times the value for momeric $BChl_a$.[21] Theoretical work has shown that the transition dipole moment of an exciton will scale as $N^{1/2}$, where N is the number of chromophores over which the exciton is delocalized.[22] For this reason, Leupold et al. concluded that the B850 excitation is delocalized over 16 ± 4 $BChl_a$ molecules, i.e., roughly over the entire ring. Circular dichroism studies have also supported the notion of a significantly delocalized exciton in B850.[7,23,24] In contrast to this, Leupold et al. found the dipole moment for emission to be considerably smaller, indicating a delocalization size of about two chromophores.[21] Similar results were obtained by Monshouwer et al. from measurements of the rate of superradiant emission.[25] Chachisvilis et al. measured the pump−probe transient absorption spectrum of B850 1.5 ps after excitation of B800 and concluded that the exciton was delocalized over 4 ± 1 $BChl_a$'s;[26] a similar study by Kennis et al. came to essentially the same conclusion.[27] By comparing pump−probe spectra (10 ps delay time) of B850 and the $BChl_a$ dimer B820, Novoderezhkin et al. concluded that the coherence length in B850 is five chromophores.[28]

At first glance it might appear that the varying estimates given above for the exciton coherence size must be in conflict with each other. However, as was pointed out very recently by Nagarajan et al.,[29] it is important to take into account the time scale spanned by the different experimental methods that have been used to determine this quantity. Absorption, hole burning and circular dichroism generally provide information on the (ultrafast) time scale of electronic dephasing. For pump−probe measurements, the time scale is set by the time delay between pump and probe pulses. In fluorescence emission studies the relevant time scale is determined by the excited-state lifetime of the system; in the case of B850 this is nearly a nanosecond.[25] As noted above, the exciton coherence size is a function of the time elapsed since the creation of the exciton.

A number of experimental studies have appeared concerning the nature of the dynamics in B850 that govern the transformation of the exciton from its initial to final state. Most of these experiments employed ultrafast one- or two-color pump−probe or pump−probe anisotropy methods.[26,27,29−37] All of these studies determined that there was significant exciton relaxation on the sub-100 fs time scale, which was generally described as exciton dephasing and/or exciton level equilibration. On the basis of photon echo peak shift data, Jimenez et al. concluded that relaxation dynamics due to thermally active vibrational modes and inhomogeneous dephasing serve to rapidly localize the electronic states of B850 to 3−4 chromophores.[38] However, because their peak shift data were unable to resolve dynamics on time scales faster than ∼60 fs, these workers were unable draw conclusions about the nature of exciton localization dynamics in B850.

Information about the coherence properties of an exciton is needed to determine its delocalization size.[15] Excitonic couplings in molecular aggregates modify the interactions between a chromophore's electronic states and the chromophore and solvent nuclear degrees of freedom.[39] Because photon echo experiments measure electronic dephasing induced by nuclear motion, such measurements can be used to observe the dynamics of exciton coherence decay.[40,41] Other ultrafast spectroscopies complement photon echo results. Transient grating and pump−probe magic angle measurements yield information on exciton population dynamics and transition dipole magnitudes, while pump−probe anisotropy data reflect dynamics of the transition dipole orientation.

In this paper, several different ultrafast coherent four-wave mixing spectroscopic methods (frequency-resolved pump−probe, frequency-resolved stimulated photo echo, photon echo peak shift, transient grating and pump−probe magic angle and anisotropy) are used to investigate the initial electronic dephasing dynamics in the LH2 complex from *Rhodobacter sphaeroides*. For comparison, monomeric $BChl_a$ in solution is examined by some of the same methods. The resulting data show that excitonic coupling leads to suppression of linear electron−nuclear coupling in B850 and that this transition's enhanced dipole moment at excitation rapidly contracts due to exciton localization. The extensively initially delocalized exciton undergoes ultrafast localization due to static disorder and vibrational dynamics. These experimental results provide essential input for theoretical models that rigorously describe exciton dynamics in light harvesting systems.[40−42] Detailed simulations

of the photon echo, transient grating and pump−probe anisotropy data and more quantitative interpretation will be presented elsewhere.[43]

II. Ultrafast Spectroscopy of Molecular Aggregates

The dynamics of molecular aggregates such as LH2 can be described by the Frenkel-exciton Hamiltonian[40,44]

$$H = \sum_n \Omega_n(q) B_n^\dagger B_n + \sum_{mn}^{m\neq n} J_{mn}(q) B_m^\dagger B_n + H_{ph} \qquad (1)$$

where Ω_n is the transition energy of chromophore n, J_{mn} describes the intermolecular coupling between two chromophores, q represents the complete set of phonon (nuclear) coordinates, H_{ph} is the phonon Hamiltonian and the operator B_n ($B_n^\dagger$) annihilates (creates) an exciton on chromophore n. Coupling between excitons and nuclear motion is incorporated through the q dependence of Ω_n and J_{mn}. Optical fields interact with the aggregate through the polarization operator

$$P = \sum_n \vec{\mu}_n (B_n + B_n^\dagger) \qquad (2)$$

where $\vec{\mu}_n$ is the transition dipole moment of chromophore n.

Time-domain optical coherence spectroscopies are currently widely used for the investigation of dynamics in condensed matter on femtosecond and picosecond time scales.[45] In commonly employed four-wave mixing experiments, a sample is irradiated with three resonant, ultrashort optical pulses. A macroscopic, third-order polarization is induced in the sample that is given by[46]

$$P^{(3)}(t,T_{23},T_{12}) \propto \int_0^\infty dt_3 \int_0^\infty dt_2 \int_0^\infty dt_1\, E(t-t_3)\, E(t-t_3-t_2)\, E(t-t_3-t_2-t_1)\, R^{(3)}(t_3,t_2,t_1) \qquad (3)$$

where $E(t)$ is the total applied electric field and $R^{(3)}$ is the third-order nonlinear optical response function. $E(t)$ is specified by

$$E(t) = E_1^*(t) e^{i(\omega t - \vec{k}_1\cdot\vec{r})} + E_2(t-T_{12}) e^{-i(\omega t - \vec{k}_2\cdot\vec{r})} + E_3(t-T_{12}-T_{23}) e^{-i(\omega t - \vec{k}_3\cdot\vec{r})} \qquad (4)$$

where E_1, E_2 and E_3 are the electric fields of the three applied pulses (an asterisk denotes the complex conjugate) with associated wavevectors $\vec{k}_1$, $\vec{k}_2$ and $\vec{k}_3$, ω is the center frequency of the laser, and T_{12} and T_{23} are the time delays between the first and second, and second and third pulses, respectively. $R^{(3)}$ consists of a sum of four terms of the form[46]

$$R^{(3)}(t_3,t_2,t_1) = \sum_{\alpha=1}^{4} [R_\alpha(t_3,t_2,t_1) - R_\alpha^*(t_3,t_2,t_1)] \qquad (5)$$

where each contribution can be expressed in terms of a four-point correlation function of the Heisenberg form of the polarization operator:

$$R_1(t_3,t_2,t_1) = \langle P(t_1)\, P(t_1+t_2)\, P(t_1+t_2+t_3)\, P(0)\rangle \qquad (6a)$$

$$R_2(t_3,t_2,t_1) = \langle P(0)\, P(t_1+t_2)\, P(t_1+t_2+t_3)\, P(t_1)\rangle \qquad (6b)$$

$$R_3(t_3,t_2,t_1) = \langle P(0)\, P(t_1)\, P(t_1+t_2)\, P(t_1+t_2+t_3)\rangle \qquad (6c)$$

$$R_4(t_3,t_2,t_1) = \langle P(t_1+t_2+t_3)\, P(t_1+t_2)\, P(t_1)\, P(0)\rangle \qquad (6d)$$

The photon echo and transient grating are two types of ultrafast three-pulse optical spectroscopies that can be expressed in terms of $P^{(3)}(t)$. For a photon echo (PE) measurement, the coherence time, T_{12}, is scanned for a fixed population time, T_{23}. PE's measure the dephasing of coherences between electronic states. In a transient grating (TG) measurement, T_{12} is set to zero and T_{23} is scanned; this technique observes the dynamics of electronic populations and nuclear coherences within those electronic states. In the most commonly used detection scheme for PE and TG measurements, the four-wave mixing signal is detected as the modulus square of $P^{(3)}$ integrated over all time t at every pair of T_{12} and T_{23} values:

$$S_{4WM}(T_{23},T_{12}) \propto \int_{-\infty}^{\infty} dt\, |P^{(3)}(t, T_{23}, T_{12})|^2 \qquad (7)$$

The photon echo peak shift (PEPS) measurement[47,48] is used to gain insight into the chromophore-solvent system−bath correlation function, which reflects interactions between the chromophore's electronic levels and the fluctuating bath, i.e., intrachromophore vibrations and solvent nuclear modes.[46] A set of PEPS data is obtained by measuring a number of photon echo profiles over a range of T_{23} times. For each profile, the position of the signal peak is recorded as a function of T_{12}. The magnitude of this "peak shift" at a given T_{23} time reflects the amount of inhomogeneous broadening present in an ensemble of chromophores on the time scale set by T_{23}; the larger the peak shift the stronger the inhomogeneous broadening. As T_{23} increases, the effective inhomogeneous broadening decreases as the ensemble loses memory of its initial configuration. The decay of the peak shift from a large initial value to a small or zero final value is therefore closely related to the system−bath correlation function.[49]

Book and Scherer have recently demonstrated that by spectrally resolving the photon echo profile information is obtained about dynamics on very fast time scales (<100 fs) that is not apparent from peak shift data.[50] This signal, the frequency-resolved stimulated photon echo (FRSPE, referred to as the wavelength-resolved stimulated photon echo or WRSPE in ref 50), is given by

$$S_{FRSPE}(\omega_D,T_{23},T_{12}) \propto \omega_D{}^2 |P^{(3)}(\omega_D,T_{23},T_{12})|^2 \qquad (8)$$

where ω_D is the detection frequency of the monochromator. $P^{(3)}(\omega_D,T_{23},T_{12})$ can be obtained by Fourier transformation of $P^{(3)}(t,T_{23},T_{12})$. It was shown in ref. 50 that contributions of vibrational coupling to the very rapid evolution of the photon echo polarization are apparent in the FRSPE signal "at a glance."

In a pump−probe measurement, a pump pulse creates (depletes) population in the electronic excited (ground) state and vibrational coherences in both the ground and excited states. A variably delayed probe then interrogates the sample and is attenuated, transmitted or amplified before it reaches a detector. In terms of the four-wave mixing formalism used in this section, fields E_1 and E_2 are both derived from the pump pulse. The probe pulse provides the E_3 interaction and also serves as a local oscillator that heterodynes the third-order polarization, yielding a signal that is sensitive to the phase of the polarization:

$$S_{pp}(T_{23}) \propto -\mathrm{Im} \int_{-\infty}^{\infty} dt\, E_3^*(t) P^{(3)}(t,T_{23},0) \qquad (9)$$

The pump−probe anisotropy (PPA) response requires that the pump−probe signal $S(t)$ be measured with the polarizations of the pump and probe oriented both parallel and perpendicular to

each other. The time-dependent anisotropy $r(t)$ is then given by

$$r(t) = \frac{S_{\|}(t) - S_{\perp}(t)}{S_{\|}(t) + 2S_{\perp}(t)} \tag{10}$$

Wynne and Hochstrasser have shown that excitonic couplings can cause $r(t)$ to differ dramatically from that of isolated chromophores.[51,52] For an isotropic ensemble of noninteracting chromophores the pump-induced anisotropy is initially 0.4 and decays to zero as a result of rotational relaxation. Coherently excited molecular dimers, however, can exhibit an initial anisotropy as high as 0.7 that decays to 0.1 as a result of dephasing and population equilibration among exciton levels.[53] These workers also predicted that the anisotropy could contain an oscillation at a frequency corresponding to the exciton splitting. This phenomenon was observed by Arnett et al. in a wavelength-resolved PPA study of the BChl dimer B820, a subunit of LH1.[54,55] These workers found a distribution of exciton splittings across the B820 absorption band which could be accounted for by assuming partially correlated inhomogeneous broadening between chromophores within a dimer. An oscillating anisotropy was also observed in the Fenna−Matthews−Olson (FMO) BChl protein[56] and the special pair of the photosynthetic reaction center.[57]

As noted in the Introduction, an important issue in the spectroscopy of light harvesting complexes is the exciton coherence size, i.e., the number of chromophores in the aggregate over which an exciton is delocalized. Meier et al. have shown that a precise definition of this quantity can made in terms of the exciton density matrix[15]

$$N_{\mathrm{mn}}(t) = \langle \tilde{B}_m^{\dagger}(t)\, \tilde{B}_n(t) \rangle \tag{11}$$

where the creation and annihilation operators are expressed in the interaction representation and the superscripts refer to chromophores n and m. The exciton coherence size is defined as the inverse participation ratio of the density matrix

$$Z(t) = \frac{\left[\sum_{mn} |N_{mn}(t)|\right]^2}{L \sum_{mn} |N_{mn}(t)|^2} \tag{12}$$

where L is the number of chromophores in the aggregate. Note that the coherence size is time-dependent (time zero is the moment of creation of the exciton) and will range from one to L, depending on the values of the off-diagonal elements of the density matrix.

III. Experimental Section

A. Sample Preparation. Bacteriochlorophyll$_a$ (Bchl$_a$, Sigma, *Rhodobacter sphaeroides*) solutions were prepared in nitrogen-purged tetrahydrofuran (THF, Fisher, optima grade). THF coordinates the Mg atom of BChl$_a$ in both axial positions, thereby producing hexacoordinated, monomeric (nonaggregated) solutions of the chromophore.[58]

To isolate LH2 complexes, wild type *Rhodobacter sphaeroides* was grown anaerobically in light as described by Vadeboncoeur et al.[59] Whole cells were suspended in 10 mM Tris−HCl, 1 mM EDTA at pH 7.8 and sonicated for 18 min at moderate amplitude (Cole Parmer Ultrasonic Homogenizer) to break the cells. The sample was centrifuged at 17000g for 15 min to remove unbroken cell debris. The supernatant containing the photosynthetic membranes was decanted and centrifuged at 245000g for 2 h. The membranes were resuspended in the Tris−EDTA buffer and 2% (w/v) 1-*O*-Octyl-β-D-glucopyranoside (BOG). Finely powdered ammonium sulfate was added with gentle stirring until precipitation occurred at a final concentration of about 10% (w/v). After centrifugation at 27000g for 10 min, the pellet was resuspended in a minimal amount of Tris−EDTA buffer and dialyzed overnight against 10 mM Tris−HCl, 1 mM EDTA and 0.8% BOG. The protein was loaded onto a DEAE−cellulose column preequilibrated with Tris−EDTA buffer containing 0.8% BOG and washed with Tris−EDTA buffer containing 0.8% BOG/0.1 M NaCl. A NaCl gradient was applied and LH2 eluted at 0.28 M NaCl. LH2-containing fractions were pooled and dialyzed overnight against Tris−HCl buffer containing 0.8% BOG and concentrated to the optical density required for four-wave mixing measurements (see below). The linear absorption spectrum of an LH2 sample is shown in Figure 1a.

B. Ultrafast Four-Wave Mixing Measurements. In ultrafast measurements of LH2, it is necessary to keep the pulse energy low to minimize the effect of exciton−exciton annihilation.[60] For this reason, the pulse intensity for LH2 samples was kept under 30 nJ/cm^2 (for BChl$_a$/THF, the intensity was ∼130 nJ/cm^2). Viewing B850 as a unit of 18 chromophores each with a frequency-independent extinction coefficient of 1.5×10^5 M^{-1} cm^{-1} (the peak absorbance for BChl$_a$ in the Q_y region), the probability for creating two excitons on a complex is then at most 9% (assuming that all of the laser spectrum overlaps the absorption band). Measurements with the power reduced by a factor of 2 (not shown) gave identical results to those presented below. The sample (peak optical density of 0.3 at 11750 cm^{-1} for LH2 and 13000 cm^{-1} for BChl$_a$/THF) was contained in a 250 μm path length spinning cell rotating at ∼10 Hz. The sample was maintained at ambient temperature and sealed from exposure to air.

Ultrashort near-infrared pulses were produced by a home-built, cavity-dumped Ti:sapphire laser (dumper positioned in the cavity's nondispersive arm) operating at repetition rates of 16−125 kHz.[61] Two different output spectra from the laser were generated by employing different sets of intracavity mirrors (Figure 1b,c, dashed lines). The first spectrum was centered at 12650 cm^{-1} (790 nm) and with a pulse width of 15 fs fwhm Gaussian, while the second was centered at 11750 cm^{-1} (850 nm) with a pulse width of 18 fs fwhm Gaussian. After exiting the cavity, the beam was sent through a pair of fused silica prisms to compensate for residual chirp on the pulse and to pre-compensate for dispersion due to a collimating lens, beam splitters, compensating plates and the front sample cell window. The pulses were nearly chirp-free, as established by transient-grating frequency resolved optical gating measurements (TG-FROG) in the self-diffraction configuration.[62] A TG-FROG trace for the pulses centered at 12650 cm^{-1} is shown in Figure 2.

A detailed description of our apparatus for measuring photon echo and transient grating signals is given elsewhere.[63] Briefly, the output of the laser was split into three beams of equal intensity and each beam was sent down a variable (beams E_1 and E_3) or fixed (E_2) optical delay line. The three input beams were arranged in the BOXCARS geometry[64] and focused into the sample with an all-reflective Cassegrain telescope (efl ∼ 30 cm) to spot sizes of ∼200 μm. At the sample, the energy per pulse was about ∼4 nJ for BChl$_a$/THF and 1 nJ or less for LH2. For magic angle pump−probe and TG measurements, an achromatic half-wave plate (Karl Lambrecht) was used to rotate the polarization of E_3 to 54.7° relative to the polarization of E_1 and E_2. The coherent four-wave mixing signal in the phase-

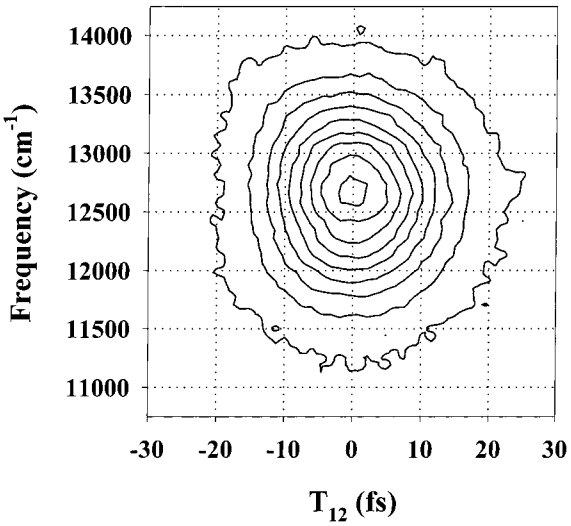

Figure 2. Transient grating frequency resolved optical gating (TG-FROG) trace of the laser pulse with a spectrum centered at 12650 cm^{-1} (790 nm). The measurement was taken in the self-diffraction configuration (identical to the three pulse stimulated echo or transient grating configuration) using neat carbon tetrachloride. The peak value of the plot is normalized to one. The value of the signal at the outermost contour is 0.04. The value at each successively inner contour increases by 0.115.

matched $\boldsymbol{k}_3 + \boldsymbol{k}_2 - \boldsymbol{k}_1$ direction was detected with an avalanche photodiode (Hamamatsu C5460). For frequency-resolved measurements, the signal was directed through a $^1/_8$ m monochromator (CVI CM110, 4 nm band-pass) prior to detection of individual spectral components.

In the PPA setup, the probe beam was generated by a reflection off a window and was sent down a variable optical delay line driven by a translation stage. The pump (<1 nJ/pulse) and probe (4% of the pump power) beams were focused into the spinning cell with a Cassegrain telescope. After the sample, the pump beam was blocked and the probe beam intensity was detected with a silicon photodiode (Centronics) and amplified. For a given measurement, a number of scans were taken with the pump polarization alternatively either parallel or perpendicular to the polarization of the probe beam. The polarization was rotated with an achromatic half wave plate.

Photon echo signals (along with the cross-correlation between E_1 and E_2) were processed with a boxcar integrator (Stanford Research Systems SR250), digitized with a digital oscilloscope (Tektronix TDS 420) and recorded in a computer via a GPIB board (National Instruments AT-GPIB/TNT). Transient grating and pump−probe signals were processed with a lock-in amplifier (Stanford Research Systems SR830) referenced to a chopper modulating the pump beam, digitized with an A-to-D board (National Instruments AT-MIO-16X) and then stored in a computer.

The instrument response function of the experimental setup was measured by filling the sample cell with a neat liquid such as carbon tetrachloride and detecting its nonresonant scattering in the same manner as the transient grating or photon echo. The TG-FROG trace (Figure 2) provides the instrument response for the FRSPE measurements. It also characterizes the chirp on the pulses to ensure that the optimum time resolution is obtained.

IV. Results

Figure 1a displays the LH2 absorption spectrum in the near-infrared region that contains the B800 and B850 bands. The

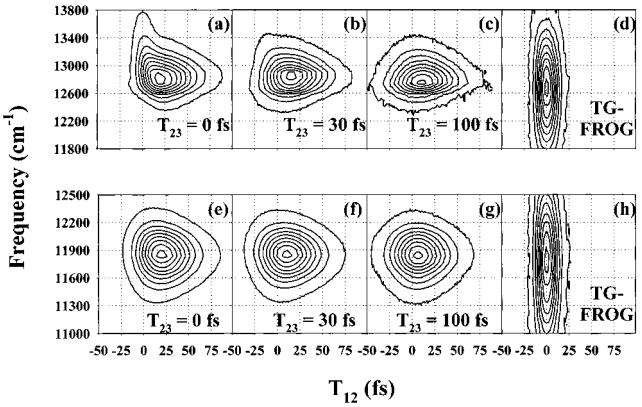

Figure 3. (a−c) Frequency-resolved stimulated photon echo signals of $BChl_a$/THF for T_{23} times of 0, 30, and 100 fs, respectively. (e−g) Frequency-resolved stimulated photon echo signals of B850 for T_{23} times of 0, 30, and 100 fs, respectively. The values of the contours follow the same pattern as in Figure 2. Associated instrument responses (TG-FROG measurements) are plotted in (d) (panels a−c) and (h) (panels e−g).

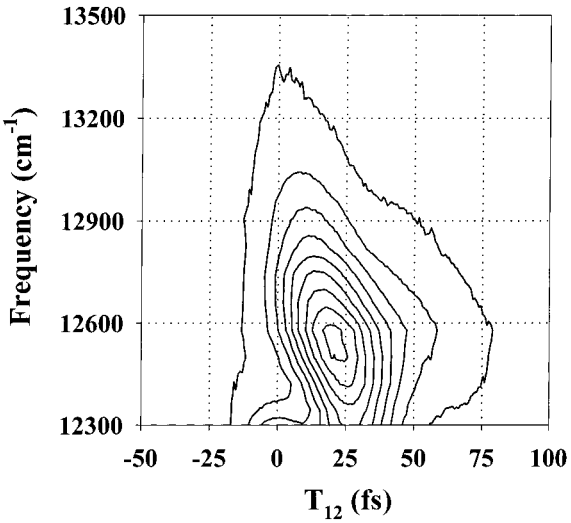

Figure 4. B800 frequency-resolved stimulated photon echo signal at $T_{23} = 0$ fs. Below 12400 cm^{-1} contributions from B850 interfere with B800 signal (see Figure 1b and text). The values of the contours follow the same pattern as in Figure 2.

dashed lines in Figure 1b,c show the two laser spectra used for the measurements presented in this paper. The solid lines in Figure 1b,c show frequency-resolved pump−probe signals for LH2 measured with the laser spectra centered at 12650 and 11750 cm^{-1}, respectively. In both of these signals, the pump and probe pulses are coincident in time. The plot in Figure 1d consists of the pump probe signal of Figure 1b divided by the square of the laser spectrum employed in the measurement. As the pump−probe signal scales as the fourth power of the applied field (cf. eqs 3 and 9), this procedure normalizes the signal for laser power across the spectrum. The resultant peak height near 12500 cm^{-1} is 3.5% of the peak height near 11750 cm^{-1}.

Figure 3a−c shows contour plots of FRSPE signals for $BChl_a$/THF at T_{23} times of 0, 30, and 100 fs, respectively. The shape of the signal as a function of T_{12} time and detection frequency evolves from an irregular shape with a "tail" feature on the high-frequency end ($T_{23} = 0$ fs) to a fairly elliptical shape ($T_{23} =$ 100 fs). Although the details differ, the overall shapes of these signals closely resemble those of the dye molecule DTTCI in methanol.[50] Figure 3d shows the TG-FROG response for comparison. Figure 4 shows the FRSPE signal for the B800 band of LH2 at $T_{23} = 0$ fs. The signal is only shown up to

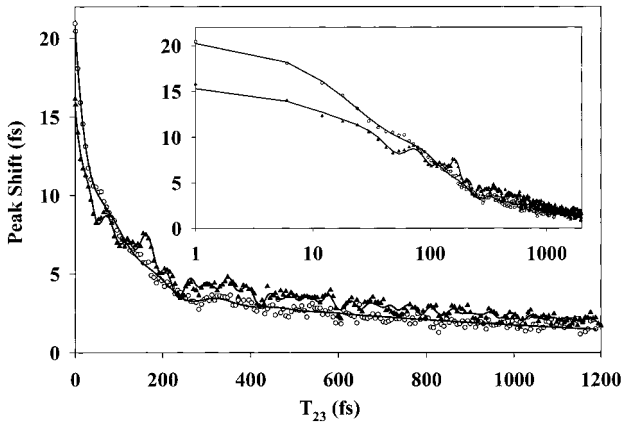

Figure 5. Photon echo peak shift data from B850 (open circles) and $BChl_a$/THF (filled triangles). The lines through the points are LPSVD fits (see Table 1 for parameters). The inset displays the data with the T_{23} axis on a logarithmic scale.

TABLE 1: LPSVD Parameters from Photon Echo Peak Shift Measurements[a]

system	A	ω (cm^{-1})	τ (fs)	ϕ (deg)
$BChl_a$/THF	10.15	0	74	0
	4.65	0	875	0
	0.81	0	>5000	0
	2.03	176	206	70.4
	1.03	338	236	91.8
	0.55	725	665	138
B850/LH2	18.63	0	63	0
	4.22	0	1136	0
	5.31	161	75	102
	1.15	256	150	166

[a] Linear prediction singular value decomposition (LPSVD) fitting parameters for photon echo peak shift (PEPS) data from B850 and $BChl_a$/THF (Figure 5). The LPSVD routine fits a signal to the form $S(t) = \Sigma_i A_i \cos(\omega_i t + \phi_i) \exp(-t/\tau_i)$, where the variables have their usual meanings.

12300 cm^{-1} because it is dominated by contributions from B850 at lower frequencies (see Figure 1b). Signals for longer T_{23} times were obscured by the energy transfer dynamics between B800 and B850.[17] This signal bears a close resemblance to the corresponding signal from monomeric $BChl_a$, including the tail feature at higher frequencies. Note the larger frequency and shorter time range for the instrument response (Figure 2 or Figure 3d) as compared with each panel in Figures 3a−c and 4. The laser spectrum was centered at 12650 cm^{-1} for these measurements.

To study the B850 band of LH2 the laser spectrum was shifted to the red so that it was peaked at 11750 cm^{-1}. Figure 3e−g shows FRSPE signals for B850 at T_{23} times of 0, 30, and 100 fs, respectively. These signals differ greatly from those of $BChl_a$ and B800. For this transition, the signal evolves from an irregular ellipse (symmetric along the frequency axis but flattened on the negative time side) at $T_{23} = 0$ fs to a near-perfect ellipse at $T_{23} = 100$ fs. There is no tail feature in the signal at $T_{23} = 0$ fs. The signal-to-noise ratio is high for this electronic transition because of its very large transition dipole moment.[21] Figure 3h shows the TG-FROG trace of the incident pulses for comparison.

Photon echo peak shift data for $BChl_a$/THF and the B850 transition are shown in Figure 5 along with linear-prediction singular value decomposition[65] (LPSVD) analyses of each trace. The LPSVD parameters are given in Table 1. The inset shows the same data on a semilog time axis. The $BChl_a$/THF peak shift data exhibit much more vibrational oscillator character and significantly smaller initial peak shift than the B850 response.

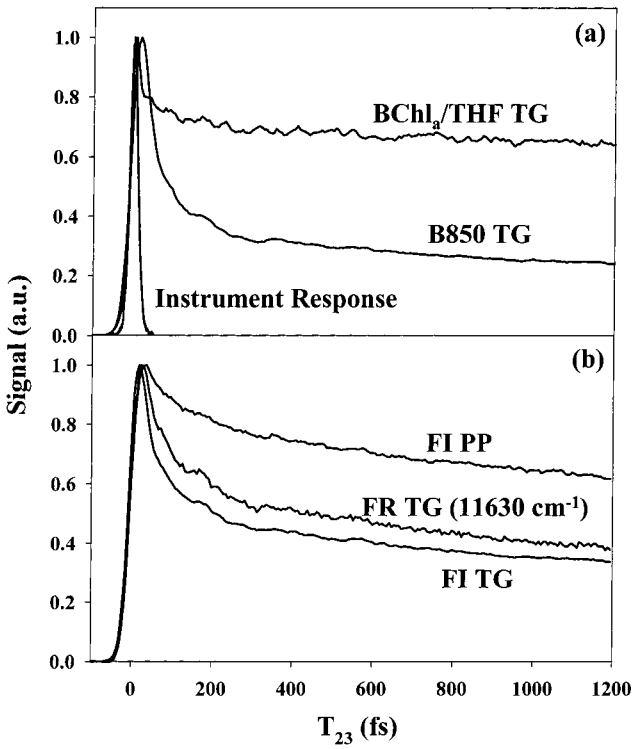

Figure 6. (a) Transient grating (TG) signals of B850 and $BChl_a$/THF. The instrument response function, measured by collecting the transient grating scattering from a nonresonant neat liquid, is also shown. (b) TG signals measured with polarization of the third beam oriented at the magic angle (54.7°) relative to the first two beams. Frequency-integrated (FI) and 11630 cm^{-1} (860 nm) frequency-resolved (FR) signals are shown, along with the FI magic angle pump−probe (PP) signal. The peaks of all signals are normalized to one.

Figure 6a shows transient grating (TG) signals for $BChl_a$/THF and B850, along with the nonresonant solvent scattering signal that determines the instrument response function. Figure 6b displays B850 transient grating signals taken with the polarization of the third pulse oriented at the magic angle relative to the first two pulses; both frequency-integrated (FI) and 11630 cm^{-1} frequency-resolved signals (FR) are shown. The frequency-integrated magic-angle pump−probe (PP) signal is also shown. In magic angle measurements, contributions to the signal from dipole moment reorientation are eliminated. The peaks of all of these signals are normalized to one. Parameters for triexponential fits to these B850 transient grating and pump−probe traces are given in Table 2. The frequency and decay time of the primary oscillation (as determined by LPSVD analysis) in each signal is also given. If exponential #1 was replaced with a Gaussian component, much poorer fits were obtained. As in the peak shift data, significantly more oscillatory character is seen in the $BChl_a$/THF results.

PPA signals (frequency-integrated and 12050 and 11800 cm^{-1} frequency-resolved) for B850 are displayed in Figure 7. The signals decay from near 0.4 to almost 0.1 and are weakly modulated by oscillations. These traces, along with those for the 11500 cm^{-1} detected signal, were fit using a nonlinear least squares routine to the sum of a Gaussian and two exponential functions:

$$S(t) = A_G \exp\left[-\left(\frac{t}{\tau_G}\right)^2\right] + A_{E1} \exp\left[\frac{-t}{\tau_{E1}}\right] + A_{E2} \exp\left[\frac{-t}{\tau_{E2}}\right] \quad (13)$$

TABLE 2: Triexponential Fits to B850 Transient Grating and Pump−Probe Measurements[a]

Frequency-Integrated TG		
exponential #1	0.567	47 fs
exponential #2	0.138	792 fs
exponential #3	0.235	>5 ps
underdamped oscillation	151 cm^{-1}	145 fs
Frequency-Integrated Magic Angle TG		
exponential #1	0.486	54 fs
exponential #2	0.353	1660 fs
exponential #3	0.159	>5 ps
underdamped oscillation	154 cm^{-1}	135 fs
11630 cm^{-1} Frequency-Resolved Magic Angle TG		
exponential #1	0.412	73 fs
exponential #2	0.344	1645 fs
exponential #3	0.242	> 5 ps
underdamped oscillation	158 cm^{-1}	202 fs
Frequency-Integrated Magic Angle PP		
exponential #1	0.154	80 fs
exponential #2	0.297	1062 fs
exponential #3	0.536	> 5 ps
underdamped oscillation	175 cm^{-1}	474 fs

[a] Triexponential fits to B850 transient grating (TG) and pump−probe (PP) measurements plotted in Figure 6. The first column for each component gives the relative amplitude while the second column gives the corresponding decay time. This fit was subtracted from the signal and the residual was analyzed with a LPSVD routine to determine the frequency and decay time of the primary underdamped oscillation in each signal.

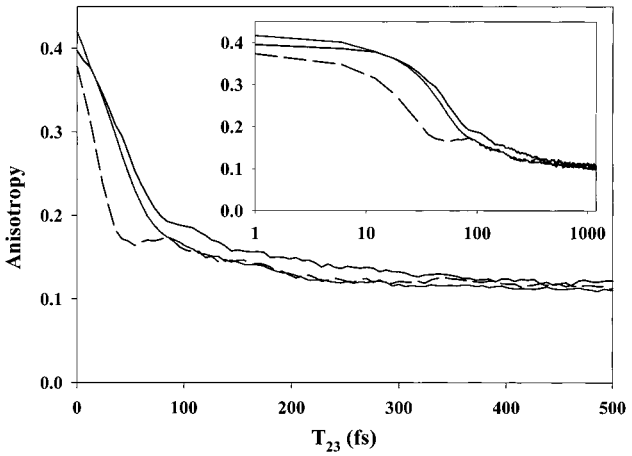

Figure 7. Pump-probe anisotropy signals of B850 detected by integration over all frequencies (uppermost solid line at T_{23} = 100 fs and beyond), detected at 12050 cm^{-1} (830 nm, dashed line) and detected at 11800 cm^{-1} (845 nm, gray line). The inset displays the data with the T_{23} axis on a logarithmic scale.

The fit was then subtracted from the signal and the residual was analyzed by LPSVD to determine the frequency and decay time of the most prominent oscillations in the signal. All fitting parameters are given in Table 3.

Figure 8 shows the frequency-resolved PPA signal across the entire B850 band for zero delay between the pump and the probe. The pump−probe signals with the probe polarization oriented both parallel and perpendicular to the pump polarization are also shown. There are divergences in the anisotropy at about 11400, 12000, 12350 cm^{-1}, where the parallel and perpendicular signals cross each other. These divergences do not reflect physically meaningful values of the anisotropy.

V. Discussion

A. Frequency-Resolved Pump−Probe. It was noted in the Introduction that the transition dipole moment of B850 for absorption has been reported to be larger than that of $BChl_a$ by

TABLE 3: Fitting Parameters for B850 Pump−Probe Anisotropy Signals[a]

Frequency-Integrated Detection		
Gaussian	0.158	52 fs
exponential #1	0.120	154 fs
exponential #2	0.117	>5 ps
underdamped oscillation	367 cm^{-1}	793 fs
12050 cm^{-1} Detection		
Gaussian	0.170	41 fs
exponential #1	0.089	140 fs
exponential #2	0.113	>5 ps
underdamped oscillation #1	241 cm^{-1}	130 fs
underdamped oscillation #2	394 cm^{-1}	108 fs
11800 cm^{-1} Detection		
Gaussian	0.176	45 fs
exponential #1	0.124	116 fs
exponential #2	0.110	>5 ps
underdamped oscillation	279 cm^{-1}	93 fs
11500 cm^{-1} Detection		
Gaussian	0.107	45 fs
exponential #1	0.130	130 fs
exponential #2	0.115	> 5 ps
underdamped oscillation	268 cm^{-1}	183 fs

[a] Fitting parameters for frequency-integrated and frequency-resolved detection of B850 pump−probe anisotropy signals. The signals were first fit to a sum of a Gaussian and two exponential functions, each characterized by an amplitude and a decay time (see eq 13). This fit was then subtracted from the signal and the residual was analyzed with a LPSVD routine to determine the frequency and decay time of the primary underdamped oscillation(s) in the signal.

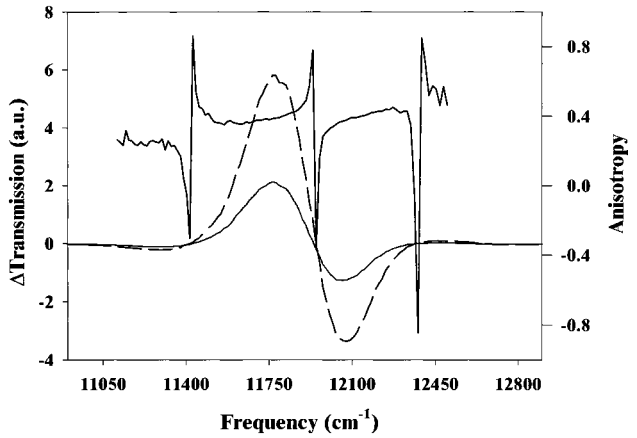

Figure 8. Frequency-resolved pump−probe anisotropy signal for B850 taken with the pump and probe pulse coincident in time (solid line, right-side axis). The pump−probe signals for the probe pulse polarization oriented parallel (dashed line) and perpendicular (gray line) to pump pulse are also shown (left-side axis).

a factor of about four,[21] which constitutes strong evidence for extensive delocalization of the initial B850 excitation.[12,22] By contrast, because the B800 $BChl_a$'s are well separated from each other, calculations predict that these chromophores should interact only weakly.[7−9] Thus, the B800 excitation can be thought of as localized on a single chromophore and its transition dipole should not be subject to enhancement.

Frequency-resolved pump−probe signals presented in Figure 1b,c provide an interesting demonstration of the relative strengths of these two transitions. For both signals, there is no time separation between the pump and the probe pulses so the initial transition moments of both bands are measured. The signal in Figure 1b was obtained with the laser spectrum centered at 12650 cm^{-1}; most of the spectrum is resonant with B800 while the tail overlaps with B850. The situation is reversed in Figure 1c, where the laser spectrum is centered at 11750

cm^{-1}. In Figure 1b the pump-induced absorptive and transmissive features of B800 (peaked at 12900 and 12500 cm^{-1}, respectively) are smaller in amplitude than the corresponding features of B850 (peaked at 12200 and 11850 cm^{-1}). This occurs despite the fact that only about 20% of the power in each pulse is at frequencies less than 12200 cm^{-1}. When the laser spectrum is shifted to the red (Figure 1c), the absorptive and transmissive features of B850 are again observed in the pump−probe signal. However, virtually no signal is observed at frequencies larger than 12350 cm^{-1} even though the tail of the laser spectrum extends beyond 13300 cm^{-1}. Because pump−probe signals scale as the fourth power of the transition dipole moment,[46] these results demonstrate that B850's dipole moment for absorption must be significantly larger than that of B800. The enhancement of this quantity in B850 is not apparent from LH2's linear absorption spectrum. Figure 1d shows the pump−probe spectrum in Figure 1b normalized for finite laser spectral width by dividing it by the square of the laser spectrum. The peak at about 11750 cm^{-1} is nearly 30 times larger than that around 12500 cm^{-1}, again demonstrating the large difference in the transition probabilities of these two bands.

These results can be used to estimate the coherence size of the initial exciton in B850. Since the exciton transition dipole moment scales as the square root of the coherence size, the ratio of the B850 to the B800 pump−probe signal scales as

$$\frac{S_{B850}}{S_{B800}} = \frac{(18/N)(N^{1/2}\mu_{BChl})^4}{9\mu_{BChl}{}^4} \qquad (14)$$

where N is the coherence size and μ_{BChl} is the transition dipole moment of a $BChl_a$ molecule. This equation assumes no exciton delocalization in B800. To determine the coherence size, the pump−probe signal in Figure 1b is fit to a sum of Gaussian functions. The functions that model the pump-induced transmission for the two bands are normalized for laser power, and then the ratio of their integrated areas are the value of the right-hand side of eq 14. Solving for N yields a value of ∼13. Given the simplicity of this analysis, we consider this estimate to be in reasonable agreement with the value of 16 determined Leupold et al.;[21] in fact, the present number is within the error bounds given by those workers.

B. Frequency-Resolved Stimulated Photon Echoes. As noted in the Results, the FRSPE signals for $BChl_a$/THF qualitatively resemble those of the dye solution DTTCI/MeOH presented in ref 50. For T_{23} times of 0 to 100 fs, the most prominent change in the FRSPE signal for both $BChl_a$ and DTTCI is the disappearance of the high-frequency tail feature (Figure 3a−c and Figure 2 of ref 50). In ref 50 it was argued that this portion of the signal is due to coupling of the electronic excitation to DTTCI's near continuum of moderate to high-frequency vibrational modes and the resultant ultrafast vibrational relaxation. Because $BChl_a$ is a large, conjugated molecule there should be significant electron−nuclear coupling in $BChl_a$ at moderate to high frequencies, similar to that of the dye molecule. Indeed, resonance Raman excitation of the Q_y transition of BChl reveals a dense spectrum of nuclear modes.[66] Therefore, the initial dephasing dynamics of $BChl_a$ and DTTCI are attributed to the same types of processes.

The FRSPE signal for B800 at $T_{23} = 0$ fs (Figure 4) qualitatively resembles that of the corresponding signal for monomeric $BChl_a$. The overall shape of the two signals are quite similar, including the high-frequency tail. This is can be explained by the fact that the nine B800 $BChl_a$'s can be considered spectroscopically isolated from one another and from the B850 $BChl_a$'s; Sauer et al. have calculated that the excitonic coupling energies between a B800 chromophore and nearby B800 and B850 chromophores are less than 15 cm^{-1}.[7] While the surrounding medium of $BChl_a$ in THF obviously differs greatly from $BChl_a$ in the LH2 protein, there is strong evidence *that initial electronic dephasing dynamics at room temperature are dominated by intramolecular dynamics.*[47,50,67] Therefore, on a time scale of 100 fs or less, it would be expected that the B800 band would give a similar FRSPE response as monomeric $BChl_a$.

In sharp contrast to B800, the FRSPE signals for the B850 transition differ greatly from those of $BChl_a$/THF (Figure 3e−g). The most prominent difference is that there is no "tail feature" in the B850 signal at $T_{23} = 0$ fs. Considering the discussion above regarding the corresponding signals for monomeric $BChl_a$ (and DTTCI), this would imply that the B850 transition is more weakly coupled to vibrational motion than the other systems. This result can be understood by considering the effect of exciton delocalization on exciton-vibration coupling. Hochstrasser and Prasad demonstrated that the intensity of the phonon sideband in the absorption spectrum of a molecular crystal varies inversely with the width of the electronic exciton bandwidth.[68] If the exciton bandwidth, the energy span of the exciton levels over all wavevectors, is sufficiently large, coupling to intramolecular modes may also be suppressed.[69] This phenomenon occurs because local nuclear motion coupled to an electronic excitation becomes increasingly averaged out as an excitation becomes increasingly delocalized. Such a mechanism was recently invoked to explain why the prominent vibronic progression in monomeric sexithiophene is absent in crystalline forms of this compound.[70] The B850 ring can be considered a molecular crystal with a one-dimensional lattice, albeit of finite extent.

The width B850 exciton one-exciton band has been calculated to be ∼1200 cm^{-1}.[7,10] Therefore, even though the excitation pulses used in the present measurements can impulsively excite modes of up to ∼1000 cm^{-1}, excitonic interactions will diminish the electron−nuclear coupling strength for all modes that can be coherently excited in these experiments. Thus, exciton delocalization causes the initial dephasing dynamics of B850 to have a significantly different character than that of B800 or monomeric $BChl_a$. While delocalization reduces the contribution of linear electron−nuclear coupling to electronic dephasing, the amplitude of thermal nuclear fluctuations will be unaffected. At room temperature thermal motion is a significant source of electronic dephasing and exciton localization.[71]

C. Photon Echo Peak Shift. Some important differences in electronic dephasing dynamics between $BChl_a$/THF and B850 are illustrated by the photon echo peak shift data for these two systems (Figure 5). The first observation to be made is that the initial peak shift of B850 (∼21 fs) is significantly larger than that of $BChl_a$/THF (∼16 fs). While the peak of the FRSPE signal for these two systems is about the same at $T_{23} = 0$ fs (Figure 3a,e), integration over the frequency axis causes the temporal location of the $BChl_a$ signal maximum to be decreased due to contributions from the high-frequency tail of the signal. This is because the tail feature is peaked at $T_{12} = 0$ fs. Note that this difference in the initial peak shift is not due to greater static inhomogenaity in B850; at $T_{23} = 1$ ps the B850 peak shift is in fact slightly larger than that of $BChl_a$/THF. The most likely explanation for this result is that the B850 excitation is more weakly coupled to its bath of nuclear modes than is the corresponding transition for monomeric $BChl_a$; the aggregate band has a longer "bath correlation time" than the monomer

and thus a larger initial peak shift.[72,73] Jimenez et al., who also measured peak shift data for B850, concluded that electron−nuclear coupling in this system was much weaker compared to carbocyanine dye molecules (such as DTTCI).[38] The conclusion to be drawn here is identical to the one reached above from the FRSPE data: exciton delocalization in B850 reduces the coupling of the electronic transition to nuclear motion.

Another observation to be drawn from the PEPS results of Figure 5 is that apart from the initial value, the time scales for the overall decay of the peak shift are comparable but not identical. This can be seen by comparing the LPSVD fitting parameters for both traces (Table 1). The different exponential decay times in the two systems reflect the differing time scales for solvation dynamics and vibrational dephasing in THF and the LH2 protein. Last, note that the amplitude of underdamped, high-frequency modes is decreased in B850 relative to $BChl_a$/THF. The prominent 338 and 725 cm^{-1} modes observed for monomeric $BChl_a$ data are absent in the B850 data (Tables 1 and 2). This is another manifestation of the effect of exciton delocalization on electron−nuclear coupling. A reduction in the intensity of high-frequency vibrational modes relative to $BChl_a$ has also been seen in PEPS data for the special pair of the photosynthetic reaction center.[74]

D. Transient Grating. Further insight into the nature of excition dynamics in B850 is revealed by comparison of the TG signals of B850 and $BChl_a$/THF (Figure 6a). For $BChl_a$ in solution, the signal consists of an initial ultrafast component followed by a slow decay modulated by high-frequency oscillations. The initial ultrafast response is attributed to the same ultrafast dynamics that are observed in the FRSPE signals of $BChl_a$/THF (Figure 3a−c), i.e., ultrafast dephasing of a quasi-continuum of medium to high-frequency vibrational modes.[50] The slower decay reflects solvation dynamics[75] while the oscillations correspond to coherently excited high-frequency vibrations. The TG signals for B850 and $BChl_a$/THF are quite different. The B850 signal is dominated by an initial ultrafast decay that accounts for more than half of the signal amplitude. The time constant of this component is 47 fs (see Table 2), significantly longer than the 22 fs instrument response function. The differences between the FRSPE signals from $BChl_a$/THF and B850 (Figure 3) show that this decay cannot be assigned to vibrational dynamics. This feature is not a "coherence spike" because it decays more slowly than the instrument response function.[76] It also cannot be due to population relaxation to the ground state or a fast Stokes shift, as the fluorescence lifetime of B850 is almost a nanosecond and the Stokes shift is less than 150 cm^{-1} (well within the laser spectral width).[25] Analogous results are obtained for pump−probe measurements on B850 and $BChl_a$/THF (not shown).

The probable origin of this 47 fs decay is the contraction of the B850 transition dipole moment due to exciton dephasing. As discussed above, the B850 transition dipole has been measured to be about four times greater than that of monomeric $BChl_a$, indicating strong delocalization at the moment of excitation.[21] Following creation of the exciton, various ultrafast dephasing mechanisms become operative and serve to diminish the exciton's enhanced dipole moment. Thermal fluctuations of nuclear degrees of freedom, which are certainly very important at room temperature, randomize the well-defined phase relationships between the monomers of aggregate.[77] Recent calculations by Kumble and Hochstrasser have explored the effects of the modest amount of static disorder believed to be present in LH2 at room temperature (inhomogeneous width of 100−200 cm^{-1}).[13] They found that this level of disorder is sufficient to cause significant dephasing on the sub-100 fs time scale by scattering the initial exciton into states with different wavevectors. Both of these dephasing processes will reduce the coherence size of the exciton and thus its transition dipole moment. The B850 TG signal in Figure 6a bears a close resemblance to the TG signal for LH1, given in Figure 4 of ref 38. This suggests that similar ultrafast exciton localization dynamics occur in both LH1 and LH2.

To separate the contribution of dipole moment contraction from that of dipole moment reorientation in the B850 signal, TG measurements were taken with the polarization of E_3 (the probe pulse) oriented at the magic angle relative to the polarizations of E_1 and E_2 (the pump pulses). Figure 6b shows frequency-integrated and 11630 cm^{-1} (860 nm) frequency-resolved TG measurements. The magic angle signals have the same overall behavior as the ordinary TG signal, although in the magic angle signals the magnitude of the initial ultrafast decay is smaller relative to the longer-time components. For comparison, the frequency-integrated magic angle pump−probe signal for B850 is also shown in Figure 6b. This signal exhibits a slower initial decay because of the linearized nature of the pump−probe measurement. These data are important constraints for simulations that attempt to rigorously model the initial and final coherence size of the B850 exciton, as well its localization dynamics. As such simulations would have to include Feynman pathways for transitions among the ground, one-exciton and two-exciton levels, fairly complicated calculations are required. The magic angle TG signal detected at 11630 cm^{-1} may prove useful in unraveling these dynamics. As can be seen in the B850 frequency-resolved pump−probe signal in Figure 1c, the third-order polarization is dominated by excited-state absorption above 12000 cm^{-1}, reflecting transitions from one-exciton to two-exciton levels. Below 12000 cm^{-1}, the signal results predominantly from stimulated emission from one-exciton levels and bleaching of the ground state. By detecting at 11630 cm^{-1}, it is ensured that the signal is dominated by transition between the ground and one-exciton levels. This TG signal may therefore be more straightforward to simulate.

E. Pump−Probe Anisotropy. Oscillatory components in PPA signals have been shown to provide information on exciton level splittings and dephasing times; examples include BChl aggregates within the B820 dimer,[54,55] reaction center[57] and FMO proteins.[56] While several groups have measured the pump−probe anisotropy of B850, to our knowledge none have reported high-frequency modes. Figure 7 shows B850 PPA signals for frequency integrated and 12050 cm^{-1} (830 nm) and 11800 cm^{-1} (845 nm) frequency-resolved detection. Fitting parameters for these traces, as well as those for 11500 cm^{-1} (870 nm) detection, are given in Table 3 (the fitting procedure is described in the Results section). All traces have initial values close to 0.4 and decay to almost 0.1 in less than a picosecond. This behavior is in agreement with results of the Sundström group[26,32] and Kennis et al.[34] However, Nagarajan et al. observed initial anisotropies greater than 0.5 when broadband excitation pulses were used.[29] The reasons for this discrepancy are not apparent unless chirp-induced coherent coupling artifacts contributed to their data.[76] For the present frequency-integrated data, the initial decay of the anisotropy occurs with a time constant of 52 fs (Table 3).

In the frequency-resolved PPA data presented here and in the work of Nagarajan et al.,[29] the initial value of the anisotropy was found to vary as a function of detection frequency. Some caution should be exercised in the physical interpretation of such results. Figure 8 shows the PPA signal detected over the entire

B850 band for zero delay between the pump and probe pulses. The pump−probe signals with the probe polarization oriented both parallel and perpendicular to that of the pump are also shown. The anisotropy shows divergences to values far from 0.4 at around 11400 cm^{-1} (875 nm), 12000 cm^{-1} (835 nm) and 12350 cm^{-1} (810 nm). At these frequencies, the parallel and perpendicular signals cross each other and are close to zero. As this is merely a numerical issue, physical meaning should not be ascribed to anisotropy values at these frequencies.

Nagarajan et al. calculated the initial frequency-resolved anisotropy of B850 following impulsive excitation for both a coherent superposition and an incoherent mixture of exciton states.[29] For the case of a coherent superposition, the calculated anisotropy is in fairly good agreement with the experimental data presented in Figure 8. In this calculation, the anisotropy is in the range of 0.35, except around 11900−12000 cm^{-1} where there is a divergence. In contrast, the anisotropy is around 0.2 when an incoherent mixture is assumed. This result provides additional evidence for an initially delocalized exciton in B850.

The LPSVD parameters given in Table 3 indicate the presence of high-frequency oscillations in the B850 PPA data. A 367 cm^{-1} mode is found in the frequency-integrated data while a 394 cm^{-1} mode is seen in the signal detected at 12050 cm^{-1}. These two frequencies are probably due to vibrational modes and not to exciton splittings, as resonance Raman[66] and low-temperature fluorescence excitation spectra[78] of monomeric $BChl_a$ show several peaks in this frequency range. In the 12050 cm^{-1} PPA signal a 241 cm^{-1} frequency is also observed. Oscillations at 279 and 268 cm^{-1} are observed in the signals detected at 11800 and 11500 cm^{-1}, respectively. The origin of these oscillations is not clear. There is some resonance Raman activity in this frequency range,[66] although it is substantially less than in the 350−400 cm^{-1} range.

While it is tempting to assign these oscillations to the coherent excitation of two exciton levels, it is not apparent that a second level exists in the B850 band with sufficient oscillator strength to manifest itself in this manner. Low-temperature hole burning measurements by Wu et al. identified the lowest exciton level of the B850 ring to be about 200 cm^{-1} below the primary transition.[79] However, it carries only 3% of the intensity of the B850 band and would be difficult to observe in our experiments. Only if diagonal disorder were significantly greater at room temperature compared to cryogenic temperatures would this transition acquire enough intensity to be readily observable.

Another possible explanation is given by the model postulated by van Oijen et al. to explain their single complex, low-temperature fluorescence excitation spectra of LH2.[19] These workers found that the spectra in the B850 region of single complexes typically contained two broad peaks with an average splitting of around 110 cm^{-1}. Measurements with oriented samples revealed that the polarization of the emission from the two peaks was mutually orthogonal. Van Oijen at al. noted that these results could be explained if it were assumed that the LH2 complexes were statically distorted from circular to elliptical geometries. The degeneracy of the B850 transition would then be lifted and two energetically distinct levels could be excited. In support of this hypothesis, a recent single-complex fluorescence study by Bopp et al. indicates that LH2 behaves like an elliptical absorber at room temperature when bound to a mica surface.[80] Analysis is underway to determine whether structural deformation of the LH2 ring is a plausible explanation of our PPA results.[43]

F. Implications for the Biological Function of LH2. Here we consider how the results presented in this paper could lead to a better understanding of the physiological operation of LH2. Following absorption of a photon by B800, energy transfer must take place to B850. The simplest way to model this process is with Förster theory,[81] where the transfer rate depends on the overlap between the donor (B800) fluorescence and acceptor (B850) absorption spectrum, and the electronic interaction between the two aggregates. The Förster rate constant can be written as[82]

$$k_{DA} = 1.18 V_{DA}^{\ 2} \int F_D(\nu)\, A_A(\nu)\, d\nu \qquad (15)$$

where k_{DA} has units of ps^{-1}, V_{DA} and ν are in cm^{-1}, and the integrated area of the fluorescence, $F_D(\nu)$, and absorption, $A_A(\nu)$, spectra are normalized to one on the cm^{-1} scale. At the lowest level of approximation, the electronic interaction matrix element, V_{DA}, is the coupling between the transition dipole moments of the donor (μ_A) and acceptor (μ_D):

$$V_{DA} = \frac{\mu_D \mu_A}{R_{DA}^3} - \frac{3(\mu_D R_{DA})(\mu_A R_{DA})}{R_{DA}^5} \qquad (16)$$

where R_{DA} is the donor−acceptor separation.

Pullerits et al. calculated the fastest feasible Förster rate assuming that transfer takes place between individual B800 and B850 $BChl_a$'s, each with a transition dipole moment of 6.4 D.[82] They determined that the time constant for this type of transfer could be no smaller than 1.9 ps. However, the B800−B850 energy transfer time has been measured to be about 700 fs.[17] Krueger et al. recently used ab initio electronic structure methods to calculate the transfer rate between one B800 and one B850 $BChl_a$ in the presence of a nearby carotenoid.[83] This much more sophisticated calculation, that did not resort to the dipole approximation, yielded a rate that was still a factor of 2 slower than experiment. Two additional mechanisms for this process have been proposed to resolve this discrepancy: transfer from B800 to an upper exciton state of B850,[82,84,85] and B800−B850 transfer enhanced by electronic mixing (superexchange interactions) with adjacent carotenoid molecules.[86,87]

Two studies have appeared very recently that approach energy transfer in LH2 in a more comprehensive way. Simulations by Scholes and Fleming demonstrated the importance of including all 18 B850 $BChl_a$'s in energy transfer simulations, but these authors contended that the dynamically localized (i.e., relaxed) exciton is the relevant acceptor state.[88] The transfer rate determined by this analysis is about half the experimental number. To match experiment, it had to be postulated that interactions with carotenoids effectively increase the coupling between B800 and B850 by 30%. Damjanovic et al. calculated the energy transfer rate using the total B850 wave function in the absence of static or dynamic disorder, which implies completely delocalized exciton states.[89] In this analysis, the $BChl_a$ electronic structure was determined by ab initio calculations including single excited configurations. As this method overestimates transition moments, and (unlike in Refs. 83 and 88) no attempt was to rescale them, the donor−acceptor coupling was significantly overestimated. For these reasons, the predicted transfer time was substantially faster than the experimental result.

In our view, the proper way to model B800−B850 energy transfer is somewhat between the two approaches discussed in the previous paragraph. It is certainly not sufficient to model the B850 acceptor as a single $BChl_a$ molecule.[82,83] The results in this paper have made it clear that an exciton in B850 is initially delocalized over the majority of the B850 aggregate.

Because no localization can occur until after B850 has been excited, it is this delocalization length that is relevant to the energy transfer process. Taking into account B850's enhanced initial transition moment would increase the calculated transfer rate by increasing the electronic interaction matrix element, V_{DA} (see eq 16). It may turn out that carotenoid interactions and/or upper exciton states do not have to be incorporated into the analysis. In such a calculation, inclusion of inhomogeneous broadening and exciton-nuclear coupling is essential to correctly determine the donor−acceptor coupling and spectral overlap. Since the B850 ring has a diameter of about 25 Å, delocalization over a considerable percentage of this structure implies a length scale that is about the same as the smallest separations between B800 and B850 chromophores. In this situation, the spatial extent of the charge distribution is nonnegligible. Therefore, the point dipole approximation[82] is not appropriate for the calculation of the B800−B850 electronic coupling; it may be necessary to determine this quantity for all orders of multipoles.[83,88,89]

An assumption typically made in energy transfer calculations is that the donor reaches thermal equilibrium in its electronically excited stated on a time scale faster than the energy transfer rate.[90] Pump−probe[91] and photon echo peak shift[74] measurements for $BChl_a$ in solution have shown that complete relaxation of the excited state following photoexcitation takes more than 20 ps; a similar result can probably be expected for B800. As the B800−B850 energy transfer rate is ∼700 fs, use of a fully relaxed emission spectrum (eq 15) for B800 in the calculation of the transfer rate may be inappropriate. A model that generalizes this theory to the case where internal relaxation of the donor takes place simultaneously with energy transfer should probably be used.[92]

While the enhanced initial transition moment of B850 may serve to increase the rate of energy transfer from B800, this property is not advantageous for storage of an electronic excitation. A large transition dipole implies a short radiative lifetime and perhaps a nonnegligible rate for back transfer. Following excitation of B850, the dipole moment of this transition rapidly contracts due to static and dynamic localization processes, ultimately to no more than twice that of the $BChl_a$ monomer.[21] The fluorescence lifetime of B850 is almost a nanosecond,[25] which leaves sufficient time for the excitation to be transferred to LH1.[93] In this view, dynamic symmetry-breaking provides positive feedback to ensure that the rate of forward transfer of the exciton (B800 to B850 to LH1) is much greater than the rates of competing processes (radiative decay or back transfer). The bath of nuclear modes serves not only as a passive source of dissipation but also actively promotes the desired transfer process.[94]

Another biological consequence of exciton delocalization may result from the suppression of linear electron−nuclear coupling in the B850 transition. This will inhibit the self-trapping of B850 excitons in a polaron-like states, which reduce exciton mobility.[71] It is probably important for an exciton localized in a portion of the B850 ring to be reasonably mobile so that it can migrate to the position on the ring that is most optimal for transfer to LH1.

VI. Conclusions

We have presented frequency-resolved pump−probe, frequency-resolved stimulated photon echo, photon echo peak shift, transient grating and pump−probe anisotropy and magic angle measurements of the B850 and B800 transitions of LH2 and monomeric $BChl_a$ in solution. Our frequency-resolved pump−probe spectra at zero delay demonstrate that the B850 transition dipole moment is significantly larger than that of B800, which implies a large initial coherence size (∼13 chromophores) for the B850 exciton. Comparison of FRSPE signals from $BChl_a$/THF and B800 shows that initial dephasing dynamics are similar in these two systems, in agreement with calculations that predict very weak couplings among the B800 monomers. The FRSPE response of B850 differs dramatically from monomeric $BChl_a$. These differences are attributed to excitonic interactions in B850 that decrease the coupling of the delocalized electronic excitation to nuclear degrees of freedom. This situation is analogous to well-understood behavior in molecular crystals. Differences in the initial photon echo peak shift values between B850 and $BChl_a$/THF are consistent with this result. While the B850 excitation is initially highly delocalized, significant localization occurs within a few hundred femtoseconds, due to thermal vibrational fluctuations and static inhomogeneous broadening. This is apparent from the comparison of the B850 and $BChl_a$/THF TG signals. The B850 TG contains a component, absent in $BChl_a$/THF, that causes the signal to decay to ∼40% of its peak value in about 175 fs. This decay is ascribed to contraction of the B850 transition dipole moment resulting from ultrafast exciton localization dynamics. Such dynamics also account for the initial decay of the PPA signal in B850. Oscillations are observed in PPA signals but they cannot yet be definitively ascribed to dynamics among exciton levels.

The discussion of the present ultrafast four-wave mixing data of LH2 has been primarily qualitative. Proper simulation of these results will require realistic modeling of the nonlinear optical response of the $BChl_a$ monomer as well as the dynamics of one- and two-exciton states of B850 that are produced by interactions among the aggregate's monomeric units. Jimenez et al.[38] simulated their B850 photon echo data with the straightforward and widely used response-function formalism developed by the Mukamel group[46] for ensembles of isolated two-level chromophores. Because $BChl_a$ has substantial excited-state absorption,[32] and because excitonic interactions are clearly of primary importance in determining the optical response of B850, such a calculation is probably not very informative and perhaps even misleading. While Jimenez et al. were able to derive a response function that could accurately reproduce their PEPS data, they did not report a simulation their TG measurement with the same parameters. Consistency between PEPS and TG results is considered to be an important test of the validity of an empirically derived response function.[47,48] Mukamel and coworkers have derived a formalism that includes all interactions and dynamical processes believed to be necessary to describe the optical response of a light harvesting complex.[40−42] The data presented in this paper should provide significant experimental constraints on this general theoretical framework to allow a comprehensive quantitative description to be developed for the ultrafast dynamics of LH2. However, the complexity of the calculations required to properly simulate exciton dynamics is significantly greater than that of a two-level system and is beyond the scope of this paper. Such an analysis in underway[43] and should considerably increase our understanding of the mechanism of light harvesting in LH2.

Acknowledgment. L.D.B is grateful to Professor Shaul Mukamel for many helpful discussions and for explaining the rigorous definition of the exciton delocalization length. We thank one of the referees for pointing out Refs. 12 and 89. This work was supported by the National Institutes of Health (RO1-8 M57768). AEO, NP, and JRN acknowledge support from the U.S. Department of Energy, Office of Basic Energy Sciences,

Division of Chemical Sciences Contract DEFG0296ER14675. Partial support from the Argonne National Laboratory-University of Chicago Collaborative Seed Grant Program (#99-014) is acknowledged. L.D.B thanks the University of Chicago for a Harper Dissertation Fellowship and N.F.S. thanks the Alfred P. Sloan and Camille and Henry Dreyfus Foundations for fellowships.

References and Notes

(1) van Grondelle, R.; Dekker: J. P.; Gillbro, T.; Sundstrom, V. *Biochim. Biophys. Acta* **1994**, *1187*, 1.

(2) Hu, X.; Ritz, T.; Damjanovic, A.; Schulten, K. *J. Phys. Chem. B* **1997**, *101*, 3854.

(3) Hu, X.; Schulten, K. *Phys. Today* **1997**, *50*, 28.

(4) Schulten, K. In *Simplicity and Complexity in Proteins and Nucleic Acids*; Frauenfelder, H., Deisenhofer, J., Wolynes, P. G., Eds.; Dahlem University Press: Berlin, 1999; Vol. p 227.

(5) Jungas, C.; Ranck, J.-L.; Rigaud, J.-L.; Joliot, P.; Verméglio, A. *EMBO J.* **1999**, *18*, 534.

(6) McDermott, G.; Prince, S. M.; Freer, A. A.; Hawthornthwaite-Lawless, A. M.; Papiz, M. Z.; Cogdell, R. J.; Issacs, N. W. *Nature* **1995**, *374*, 517.

(7) Sauer, K.; Cogdell, R. J.; Prince, S. M.; Freer, A.; Issacs, N. W.; Scheer, H. *Photochem. Photobiol.* **1996**, *64*, 564.

(8) Freer, A.; Prince, S.; Sauer, K.; Papiz, M.; Hawthornthwaite-Lawless, A.; McDermott, G.; Cogdell, R.; Issacs, N. W. *Structure* **1996**, *4*, 449.

(9) Alden, R. G.; Johnson, E.; Nagarajan, V.; Parson, W. W.; Law, C. J.; Cogdell, R. G. *J. Phys. Chem. B* **1997**, *101*, 4667.

(10) Linnanto, J.; Korppi-Tommola, J. E. I.; Helenius, V. M. *J. Phys. Chem. B* **1999**, *103*, 8739.

(11) Sturgis, J. N.; Robert, B. *Photosyn. Res.* **1996**, *50*, 5.

(12) Cory, M. G.; Zerner, M. C.; Hu, X.; Schulten, K. *J. Phys. Chem. B* **1998**, *102*, 7640.

(13) Kumble, R.; Hochstrasser, R. M. *J. Chem. Phys.* **1998**, *109*, 855.

(14) Leegwater, J. A. *J. Phys. Chem.* **1996**, *100*, 14403.

(15) Meier, T.; Chernyak, V.; Mukamel, S. *J. Phys. Chem. B* **1997**, *101*, 7332.

(16) Kühn, O.; Sundström, V. *J. Chem. Phys.* **1997**, *107*, 4154.

(17) Sundström, V.; Pullerits, T.; van Grondelle, R. *J. Phys. Chem. B* **1999**, *103*, 2327.

(18) Reddy, N. R. S.; Small, G. J.; Siebert, M.; Picorel, R. *Chem. Phys. Lett.* **1991**, *181*, 391.

(19) van Oijen, A. M.; Ketelaars, M.; Köhler, J.; Aartsma, T. J.; Schmidt, J. *Science* **1999**, *285*, 400.

(20) Knapp, E. W. *Chem. Phys.* **1984**, *85*, 73.

(21) Leupold, D.; Stiel, H.; Teuchner, K.; Nowak, F.; Sandner, W.; Ücker, B.; Scheer, H. *Phys. Rev. Lett.* **1996**, *77*, 4675.

(22) Spano, F. C.; Mukamel, S. *Phys. Rev. A* **1989**, *40*, 5783.

(23) Koolhaas, M. H. C.; van der Zwan, G.; Frese, R. N.; van Grondelle, R. *J. Phys. Chem. B* **1997**, *101*, 7262.

(24) Koolhaas, M. H. C.; Frese, R. N.; Fowler, G. J. S.; Bibby, T. S.; Georgakopoulou, S.; van der Zwan, G.; Hunter, C. N.; van Grondelle, R. *Biochemistry* **1998**, *37*, 4693.

(25) Monshouwer, R.; Abrahamsson, M.; van Mourik, F.; van Grondelle, R. *J. Phys. Chem. B* **1997**, *101*, 7241.

(26) Chachisvilis, M.; Kuhn, O.; Pullerits, T.; Sundström, V. *J. Phys. Chem. B* **1997**, *101*, 7275.

(27) Kennis, J. T. M.; Streltsov, A. M.; Permentier, H.; Aartsma, T. J.; Amsesz, J. *J. Phys. Chem. B* **1997**, *101*, 8369.

(28) Novoderezhkin, V.; Monoshouwer, R.; van Grondelle, R. *J. Phys. Chem. B* **1999**, *103*, 10540.

(29) Nagarajan, V.; Johnson, E. T.; Williams, J. C.; Parson, W. W. *J. Phys. Chem. B* **1999**, *103*, 2297.

(30) Kennis, J. T. M.; Streltsov, A. M.; Aartsma, T. J.; Nozawa, T.; Amesz, J. *J. Phys. Chem.* **1996**, *100*, 2438.

(31) Pullerits, T.; Chachisvilis, M.; Jones, M. R.; Hunter, C. N.; Sundström, V. *Chem. Phys. Lett.* **1994**, *224*, 355.

(32) Pullerits, T.; Chachisvilis, M.; Sundström, V. *J. Phys. Chem.* **1996**, *100*, 10787.

(33) Savikhin, S.; Struve, W. S. *Chem. Phys.* **1996**, *210*, 91.

(34) Kennis, J. T. M.; Streltsov, A. M.; Vulto, S. I. E.; Aartsma, T. J.; Nozawa, T.; Amesz, J. *J. Phys. Chem. B* **1997**, *101*, 7827.

(35) Freiberg, A.; Jackson, J. A.; Lin, S.; Woodbury, N. W. *J. Phys. Chem. A* **1998**, *102*, 4372.

(36) Nagarajan, V.; Alden, R. G.; Williams, J. C.; Parson, W. W. *Proc. Natl. Acad. Sci. U.S.A.* **1996**, *93*, 13774.

(37) Vulto, S. I. E.; Kennis, J. T. M.; Streltsov, A. M.; Amesz, J.; Aartsma, T. J. *J. Phys. Chem. B* **1999**, *103*, 878.

(38) Jimenez, R.; van Mourik, F.; Yu, J. Y.; Fleming, G. R. *J. Phys. Chem. B* **1997**, *101*, 7350.

(39) Scherer, P. O. J.; Fischer, S. F. *Chem. Phys.* **1984**, *86*, 269.

(40) Meier, T.; Chernyak, V.; Mukamel, S. *J. Chem. Phys.* **1997**, *107*, 8759.

(41) Zhang, W. M.; Meier, T.; Chernyak, V.; Mukamel, S. *J. Chem. Phys.* **1998**, *108*, 7763.

(42) Chernyak, V.; Zhang, W. M.; Mukamel, S. *J. Chem. Phys.* **1998**, *109*, 9587.

(43) Book, L. D.; Mukamel, S.; Scherer, N. F., work in progress.

(44) Davydov, A. S. *Theory of Molecular Excitons*; Plenum Press: New York, 1971.

(45) *Ultrafast Phenomena XI*; Elsaesser, T., Fujimoto, J. G., Wiersma, D. A., Zinth, W., Eds.; Springer-Verlag: Berlin, 1998.

(46) Mukamel, S. *Principles of Nonlinear Optical Spectroscopy*; Oxford University Press: New York, 1995.

(47) de Boeij, W.; Pshenichnikov, M. S.; Wiersma, D. A. *J. Phys. Chem.* **1996**, *100*, 11806.

(48) Joo, T.; Jia, Y.; Yu, J.-Y.; Lang, M. J.; Fleming, G. R. *J. Chem. Phys.* **1996**, *104*, 6089.

(49) de Boeij, W. P.; Pshenichnikov, M. S.; Wiersma, D. A. *Chem. Phys. Lett.* **1996**, *253*, 53.

(50) Book, L. D.; Scherer, N. F. *J. Chem. Phys.* **1999**, *111*, 792.

(51) Wynne, K.; Hochstrasser, R. M. *Chem. Phys.* **1993**, *171*, 179.

(52) Wynne, K.; Hochstrasser, R. M. *J. Raman Spectrosc.* **1995**, *26*, 561.

(53) Galli, C.; Wynne, K.; LeCours, S. M.; Therien, M. J.; Hochstrasser, R. M. *Chem. Phys. Lett.* **1993**, *206*, 493.

(54) Arnett, D. C.; Kumble, R.; Visschers, R. W.; Dutton, P. L.; Hochstrasser, R. M.; Scherer, N. F. *J. Phys. Chem. B*, submitted for publication.

(55) Arnett, D. C.; Kumble, R.; Visschers, R. W.; Moser, C. C.; Dutton, P. L.; Hochstrasser, R. M.; Scherer, N. F. *Proc. SPIE* **1998**, *3273*, 244.

(56) Savikhin, S.; Buck, D. R.; Struve, W. S. *Chem. Phys.* **1997**, *223*, 303.

(57) Arnett, D. C.; Moser, C. C.; Dutton, P. L.; Scherer, N. F. *J. Phys. Chem. B* **1999**, *103*, 2014.

(58) Connolly, J. S.; Samuel, E. B.; Janzen, A. F. *Photochem. Photobiol.* **1982**, *36*, 565.

(59) Vadeboncoeur, C.; Mamet-Bratley, M.; Gingras, G. *Biochemistry* **1979**, *18*, 4308.

(60) Bradforth, S. E.; Jimenez, R.; van Mourik, F.; van Grondelle, R.; Fleming, G. R. *J. Phys. Chem.* **1995**, *99*, 16179.

(61) Liau, Y.-H.; Unterreiner, A. N.; Arnett, D. C.; Scherer, N. F. *Appl. Opt.* **1999**, *38*, 7386.

(62) Sweetser, J. N.; Fittinghoff, D. N.; Trebino, R. *Opt. Lett.* **1997**, *22*, 519.

(63) Book, L. D.; Arnett, D. C.; Scherer, N. F. *J. Chem. Phys.*, in press (2000).

(64) Eckbreth, A. C. *Appl. Phys. Lett.* **1978**, *32*, 421.

(65) Barkhuisjen, H.; de Beer, R.; Bovee, W. M. M. J.; van Ormondt, J. *J. Magn. Reson.* **1985**, *61*, 465.

(66) Diers, J. R.; Bocian, D. F. *J. Am. Chem. Soc.* **1995**, *117*, 6629.

(67) Nagasawa, Y.; Passino, S. A.; Joo, T.; Fleming, G. R. *J. Chem. Phys.* **1997**, *106*, 4840.

(68) Hochstrasser, R. M.; Prasad, P. N. *J. Chem. Phys.* **1972**, *56*, 2814.

(69) Craig, D. P.; Dissado, L. A. *Chem. Phys.* **1976**, *14*, 89.

(70) Horowitz, G.; Valat, P.; Garnier, F.; Kouki, F.; Wintgens, V. *Opt. Mater.* **1998**, *9*, 46.

(71) Meier, T.; Zhao, Y.; Chernyak, V.; Mukamel, S. *J. Chem. Phys.* **1997**, *107*, 3876.

(72) Cho, M.; Yu, J.-Y.; Joo, T.; Nagasawa, Y.; Passino, S. A.; Fleming, G. R. *J. Phys. Chem.* **1996**, *100*, 11944.

(73) Jordanides, X. J.; Lang, M. J.; Song, X.; Fleming, G. R. *J. Phys. Chem. B* **1999**, *103*, 7995.

(74) Arnett, D. C.; Book, L. D.; Moser, C. C.; Dutton, P. L.; Scherer, N. F. *J. Phys. Chem. B*, submitted for publication.

(75) Horng, M. L.; Gardecki, J. A.; Papazyan, A.; Maroncelli, M. *J. Phys. Chem.* **1995**, *99*, 17311.

(76) Oudar, J.-L. *IEEE J. Quantum Electron.* **1983**, *QE−19*, 713.

(77) Spano, F. C.; Kuklinski, J. R.; Mukamel, S. *Phys. Rev. Lett.* **1990**, *65*, 211.

(78) Renge, I.; Mauring, K.; Avarmaa, R. *J. Lumin.* **1987**, *37*, 207.

(79) Wu, H.-M.; Reddy, N. R. S.; Small, G. J. *J. Phys. Chem. B* **1997**, *101*, 651.

(80) Bopp, M. A.; Sytnik, A.; Howard, T. D.; Cogdell, R. J.; Hochstrasser, R. M. *Proc. Natl. Acad. Sci. U.S.A.* **1999**, *96*, 11271.

(81) Förster, T. *Naturwissenschaften* **1946**, *33*, 166.

(82) Pullerits, T.; Hess, S.; Herek, J. L.; Sundström, V. *J. Phys. Chem. B* **1997**, *101*, 10560.

(83) Krueger, B. P.; Scholes, G. D.; Fleming, G. R. *J. Phys. Chem. B* **1998**, *102*, 5378.

(84) Wu, H.-M.; Savikhin, S.; Reddy, N. R. S.; Jankowiak, R.; Cogdell, R. J.; Struve, W. S.; Small, G. J. *J. Phys. Chem.* **1996**, *100*, 12022.
(85) Kühn, O.; Sundström, V. *J. Phys. Chem. B* **1997**, *101*, 3432.
(86) Koepke, J.; Hu, X.; Muenke, C.; Schulten, K.; Michel, H. *Structure* **1996**, *4*, 581.
(87) Scholes, G. D.; Harcourt, R. D.; Fleming, G. R. *J. Phys. Chem. B* **1997**, *101*, 7302.
(88) Scholes, G. D.; Fleming, G. R. *J. Phys. Chem. B* **2000**, *104*, 1854.
(89) Damjanovic, A.; Ritz, T.; Schulten, K. *Phys. Rev. E* **1999**, *59*, 3293.
(90) Laible, P. D.; Knox, R. S.; Owens, T. G. *J. Phys. Chem. B* **1998**, *102*, 1641.
(91) Becker, M.; Nagarajan, V.; Parson, W. W. *J. Am. Chem. Soc.* **1991**, *113*, 6840.
(92) Mukamel, S.; Rupasov, V. *Chem. Phys. Lett.* **1995**, *242*, 17.
(93) Nagarajan, V.; Parson, W. W. *Biochemistry* **1997**, *36*, 2300.
(94) Cápek, V.; Tributsch, H. *J. Phys. Chem. B* **1999**, *103*, 3711.